Lithos 268–271 (2017) 1–15

Contents lists available at ScienceDirect

Lithos

journal homepage: www.elsevier.com/locate/lithos

Layering in peralkaline magmas, Ilímaussaq Complex, S Greenland

Emma J. Hunt *[,1], Adrian A. Finch, Colin H. Donaldson

Department of Earth & Environmental Sciences, University of St Andrews, Irvine Building, St Andrews, Fife KY16 9AL, UK

ARTICLE INFO

Article history:
Received 9 May 2016
Accepted 24 October 2016
Available online 29 October 2016

Keywords:
Ilímaussaq Complex
Kakortokite
Agpaitic
Macrorhythmic layering
Crystal size distribution
Eudialyte-group minerals

ABSTRACT

The peralkaline to agpaitic Ilímaussaq Complex, S. Greenland, displays spectacular macrorhythmic (>5 m) layering via the kakortokite (agpaitic nepheline syenite), which outcrops as the lowest exposed rocks in the complex. This study applies crystal size distribution (CSD) analyses and eudialyte-group mineral chemical compositions to study the marker horizon, Unit 0, and the contact to the underlying Unit −1. Unit 0 is the best-developed unit in the kakortokites and as such is ideal for gaining insight into processes of crystal formation and growth within the layered kakortokite. The findings are consistent with a model whereby the bulk of the black and red layers developed through in situ crystallisation at the crystal mush–magma interface, whereas the white layer developed through a range of processes operating throughout the magma chamber, including density segregation (gravitational settling and flotation). Primary textures were modified through late-stage textural coarsening via grain overgrowth. An open-system model is proposed, where varying concentrations of halogens, in combination with undercooling, controlled crystal nucleation and growth to form Unit 0. Our observations suggest that the model is applicable more widely to the layering throughout the kakortokite series and potentially other layered peralkaline/agpaitic rocks around the world.

1. Introduction

The Ilímaussaq Complex, ~1160 ± 2 Ma (Waight et al., 2002), is a peralkaline to agpaitic[2] layered intrusion characterised by spectacular mineral assemblages. It forms part of the Gardar igneous province (1.35–1.14 Ga, Upton, 2013) of South Greenland, which is comprised of: central complexes predominantly composed of syenite; mafic to intermediate dyke swarms; 'giant dykes' up to 800 m in width (Upton, 2013), composed of syenogabbro with granitic or syenitic centres; and basin fill sequences of clastic sediments with sub-aerial lavas (Upton et al., 2003). Many Gardar central complexes are marked by the development of igneous layering, in the form of modal layering, phase layering, cryptic layering and igneous lamination (Upton et al., 1996). The modal layering is often present as dominantly feldspathic sequences with subordinate mafic layers and a range of processes have been invoked to account for its development. These include: density segregation of the mafic crystals from the felsic during gravitational settling; in situ growth following intermittent suppression of feldspar nucleation; settling of 'cumulate rafts' through the host magma; and flotation of cumulates (see Upton et al., 1996 for a comprehensive review).

The Ilímaussaq Complex has some of the most spectacular layering in the Gardar Province, within its agpaitic rocks. The complex is subdivided into an outer sheath of augite syenite, which encloses the alkali granite then pulaskite, foyaite and sodalite foyaite that form part of the roof series. The bulk of the complex comprises agpaitic nepheline syenites, which from the roof down are: naujaite (oikocrystic sodalite-rich nepheline syenite); lujavrite (a melanocratic, laminated nepheline syenite rich in aegirine or arfvedsonite); and the lowermost exposed rocks are 'kakortokites' (Fig. 1), which are the focus of the present study. Many of the rock names within the present study are repeated from early work on the complex, i.e. by Giesecke in 1806 and 1809 and Ussing in 1900 and 1908 (referenced within Sørensen, 2001), thus many are unique. The term kakortokite refers to a sequence of repetitively layered nepheline syenites, distinguished by tripartite units. Each unit has a lower layer rich in arfvedsonite (black kakortokite), overlain by eudialyte-rich rocks (red kakortokite) then by alkali feldspar-rich rocks (white kakortokite). These rocks include REE-, Zr-, Nb- and Ta-rich eudialyte, which is currently attracting economic interest.

The layering in the Ilímaussaq kakortokites is notably different from most layering found elsewhere in the Gardar Province, which is interpreted to be associated with F-rich, low viscosity magmas (e.g. Parsons and Butterfield, 1981). Most igneous layering in the Gardar is characterised by fine (centimetre- to metre-scale) layers with cross-cutting relationships in the form of channels and slumps, which are formed by convecting magmas (Upton, 2013). The layering in the kakortokites is by contrast remarkably homogeneous across the entire outcrop (10 km^2; Fig. 2a–b) and cross-cutting relationships are absent,

* Corresponding author.
E-mail address: emma.hunt@wits.ac.za (E.J. Hunt).
[1] Present address: School of Geosciences, University of the Witwatersrand, Private Bag 3, 2050 Wits, South Africa.
[2] The term 'agpaitic' refers to highly peralkaline nepheline syenite characterised by complex Zr- and Ti-silicates such as eudialyte, aenigmatite and/or rinkite (Sørensen, 1997).

http://dx.doi.org/10.1016/j.lithos.2016.10.023

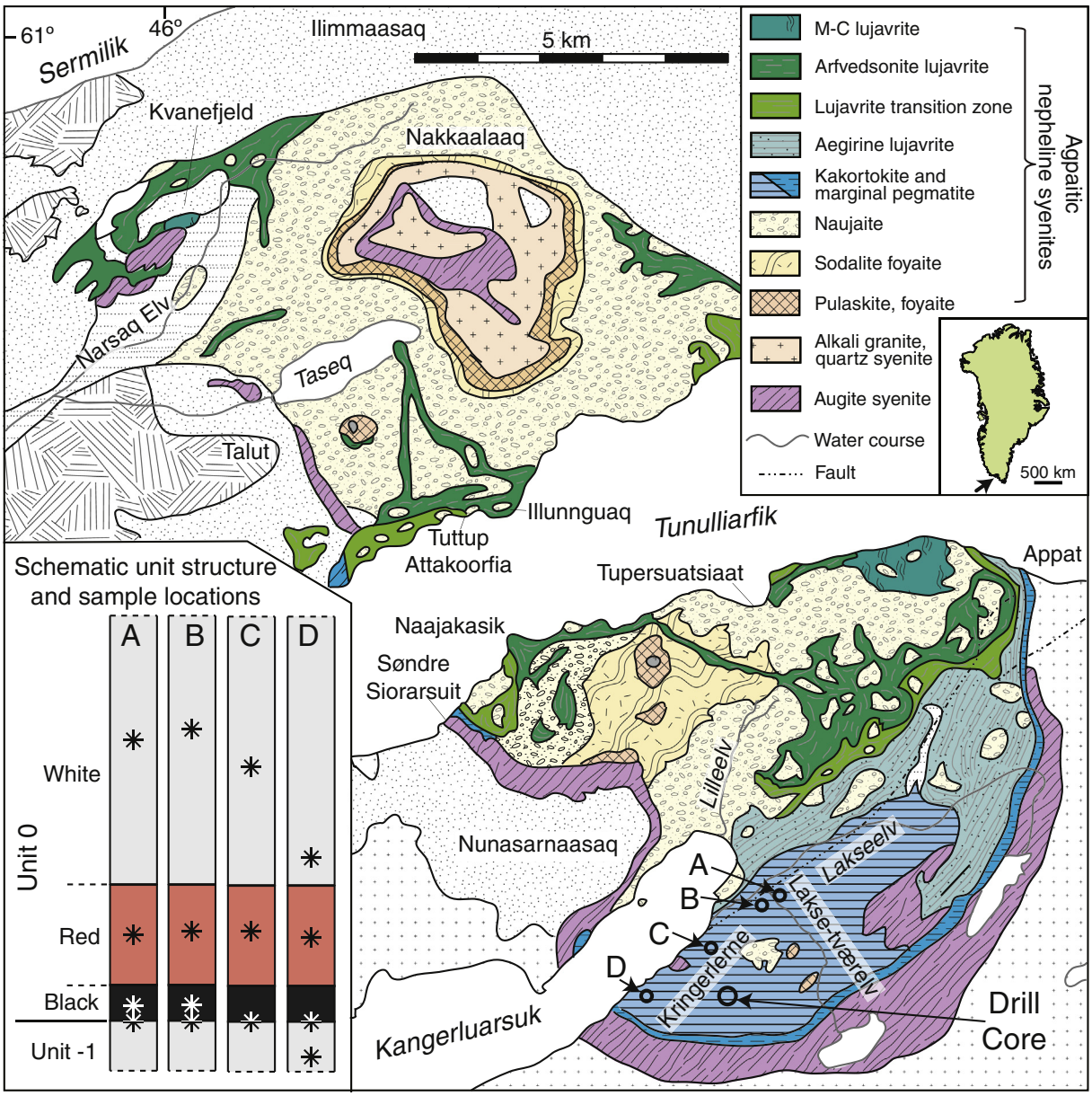

Fig. 1. Sketch map of the Ilímaussaq Complex modified after Sørensen (2001), indicating sample locations. Inset (bottom left) of schematic stratigraphic columns indicates approximate stratigraphic height of samples from each location.

except at the margins of the complex. Layering is macrorhythmic (mean unit thickness of 7 m) and 29 outcropping units have been distinguished and numbered −11 to +17, relative to the best-developed unit, the Unit 0 marker horizon, which outcrops towards the middle (in the vertical sense) of the layered series (Fig. 2a–b; Bohse et al., 1971). Autoliths petrologically and chemically consistent with the roof rocks (Steenfelt and Bohse, 1975) are incorporated within Unit +3, and one particularly large example (Fig. 2b) compresses the units below. Unit +4 is draped over the autolith (e.g. Larsen and Sørensen, 1987). These autoliths are inferred to have separated from the roof sequence during a single roof collapse event, providing evidence for development of the kakortokites through upwards accretion via large-scale processes that operated across the entire magma chamber floor (Larsen and Sørensen, 1987).

The mechanism for the formation of the layering in the kakortokite sequence remains undetermined. Most hypotheses invoke gravitational settling and density sorting (e.g. Bohse et al., 1971; Bons et al., 2015; Ferguson, 1964; Larsen and Sørensen, 1987; Ussing, 1912). However, Pfaff et al. (2008) concluded that the thickness of the overlying magma in the chamber was insufficient for the segregation of the individual layers, of at least the upper units, through gravitational settling alone. The present study combines detailed petrographic analyses, crystal size distributions (CSDs) and eudialyte crystal compositions to provide an insight into processes of development of igneous rocks. The CSD method has been applied over the last ~30 years to mafic rocks to provide a quantitative insight into processes of nucleation and crystal growth during solidification (e.g. Boorman et al., 2004; Marsh, 1988, 1998). To the authors' knowledge, this is the first time the technique has been applied to agpaitic nepheline syenites, thus allowing for greater insight into the development of the kakortokites. Unit 0 was chosen for these analyses as it is a readily identifiable marker horizon across the kakortokite series (the red layer is particularly well developed), demonstrating that samples taken laterally across several km indeed relate to the same unit. Our study provides an insight into one of the world's most spectacular and enigmatic layered intrusions and provides an understanding of the mechanisms that operate in a low viscosity, volatile-rich agpaitic magma.

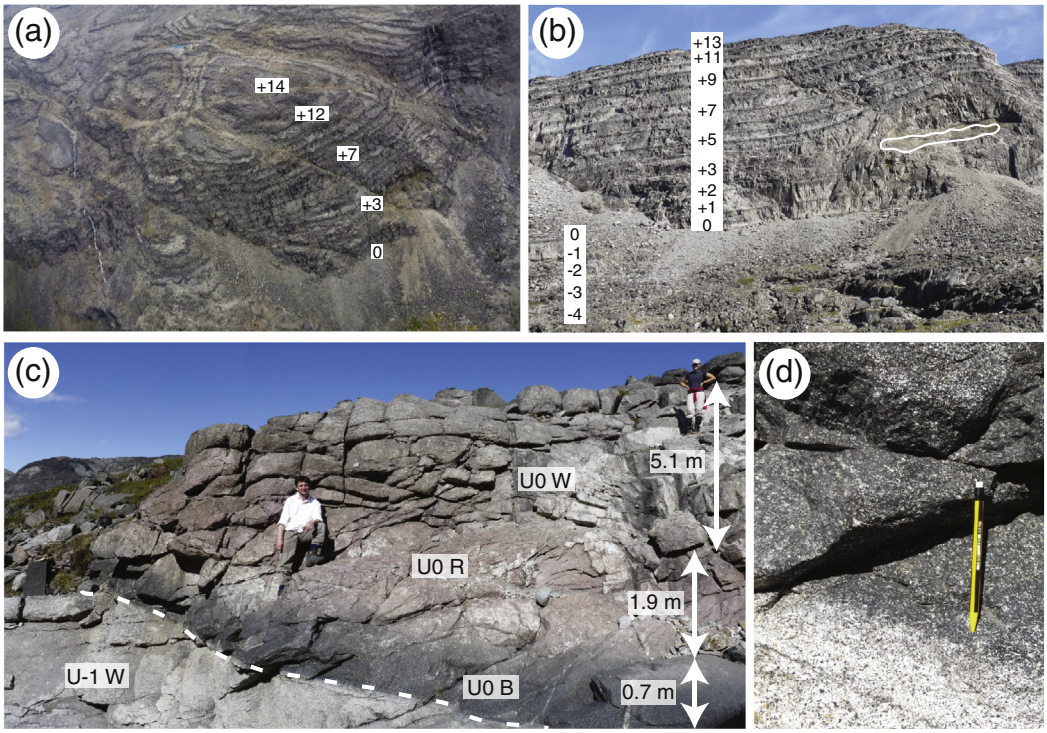

Fig. 2. (a) Aerial view of layered kakortokite from Unit 0 to Unit +16 in Kringlerne Plateau. Typical vertical differences between layers are ~7 m. (b) Units −4 to +13 outcropping in cliff face. Outlined in white is the large roof rock autolith included in Unit +3. (c) Unit 0 in outcrop. Dashed line indicates sharp Unit −1/Unit 0 boundary with the thicknesses of layers indicated. (d) Sharp, planar contact from Unit −1 white to Unit 0 black. Pencil for scale = 14 cm.

2. Field characteristics

Field data reported in this study were collected during fieldwork in the summers of 1999 and 2012, the latter with the assistance of the exploration company TANBREEZ Mining Greenland A/S. Samples are now in the collections of the University of St Andrews. Black, red and white kakortokites were sampled from Unit 0 at four locations (Fig. 1), and samples were also taken across the underlying Unit −1/Unit 0 boundary, to represent the centre to the margin of the layered sequence. Full sample descriptions are shown in Table 1 and depicted in Figs. SF1 and SF2 in the supplementary files.

The textures (i.e. strength of fabric) and thicknesses of each of the black, red and white layers vary from unit to unit (e.g. Bohse et al., 1971). However, each is remarkably homogeneous along outcrop and in drill core. Unit 0 is noted for its conspicuous red layer, although black, red and white layers are present in all units. Unit 0 is well developed and regarded as representative of the units of the kakortokite sequence in general.

Unit 0 is laterally continuous and can be traced for over 5 km; it is remarkably uniform in thickness, texture and composition across the entire outcrop (Fig. 2). At all exposures, the boundary between the Unit −1 white kakortokite to the Unit 0 black kakortokite is sharp and planar

Table 1
Description of samples according to locality and brief petrographical descriptions, see also Figs. SF1 & SF2 for section photomicrographs. Alteration refers to decomposition of eudialyte to nacareniobsite-Ce, catapleiite, pectolite and britholite. Abbreviations: Aeg — aegirine, arfv — arfvedsonite, eud — eudialyte, fsp — alkali feldspar, neph — nepheline, sod — sodalite.

Location	Sample no.	Unit	Petrography (modal %)
A	EJH/12/010	U0 white	Fsp groundmass, 47%, defines foliation. 25% arfv, 15% neph, 8% eud, 5% sod.
60.8811982°, −45.8290141°	EJH/12/007	U0 red	Eud groundmass, 59%. 12% fsp (defines a foliation fabric), 10% neph, 7% arfv, 7% aeg, 5% sod.
	EJH/12/008	U0 black	Arfv groundmass, 48%, some phenocrysts. 23% fsp, 22% neph, 5% eud, 2% sod.
	EJH/12/009	U-1/0	U0 black: arfv groundmass, 55%, some phenocrysts. 22% fsp (commonly embayed, defines foliation), 16% neph, 5% eud, 2% sod. U-1 white: fsp groundmass, 45%, defines foliation, some embayed. 20% neph, 20% arfv, 8% eud, 5% aeg, 2% sod.
B	AF/99/191	U0 white	Fsp groundmass, 49%, defines foliation. 20% neph, 19% arfv, 6% aeg, 6% eud, 1% sod.
60.88124°, −45.83117°	AF/99/193	U0 red	Eud groundmass, 55%, patchy alteration. 15% aeg, 14% neph, 10% fsp, 4% arfv, 2% sod.
	AF/99/192	U0 black	Arfv groundmass, 50%, some phenocrysts. 22% fsp, 17% eud, 11% neph, <1% sod.
	AF/99/195	U-1/0	U0 black: arfv groundmass, 54%. 20% fsp (embayed, defines foliation), 14% neph, 6% eud, 4% sod, 2% aeg. U-1 white: groundmass of fsp (34%, defines foliation) and neph (30%). 10% aeg, 10% sod, 8% eud, 8% arfv.
C	EJH/12/096	U0 white	Neph groundmass, 45%, completely altered. 18% fsp (defines foliation), 15% eud, 12% arfv, 6% aeg, 4% sod.
60.8742492°, −45.8473802°	EJH/12/095	U0 red	Eud groundmass, 50% (80% of which altered at margins). 22% fsp, 18% aeg, 10% neph.
	EJH/12/094	U-1/0	U0 black: arfv groundmass, 61%, some phenocrysts. 18% fsp (often signs of resorption, defines foliation), 15% nepheline (some altered), 6% altered eud. U-1 white: fsp groundmass, 48%, defines foliation. 18% neph, 16% aeg, 10% eud, 8% arfv
D	EJH/12/082	U0 white	Neph groundmass, 55%. 15% fsp (defines foliation), 13% arfv, 8% aeg, 7% eud, 2% sod.
60.8657099°, −45.8613828°	EJH/12/080	U0 red	Eud groundmass, 48%, minor alteration at margins. 18% fsp, 15% arfv, 12% sod, 5% neph, 3% aeg.
	EJH/12/079	U-1/0	U0 black: arfv groundmass, 72%. 14% fsp (often signs of resorption), 10% neph, 4% eud. U-1 white: sod groundmass, 42%. 20% fsp (defines foliation), 14% aeg, 10% arfv, 8% eud, 6% neph (altered).
	EJH/12/081	U-1 white	Fsp groundmass, 50%, defines foliation. 20% arfv, 15% neph, 8% eud, 5% aeg, 2% sod.

(Fig. 2c–d), whereas the intra-unit boundaries are gradational over 2 to 5 cm (Fig. 2c). The thickness of the unit is relatively constant across four outcropping locations and drill cores (access provided by TANBREEZ). It is 7.8 m thick, of which the first 0.7 m is black kakortokite, overlain by 1.9 m of red kakortokite and then by 5.1 m of white kakortokite (Fig. 2c).

There is no evidence for magma flow in the centre of the kakortokite series, by which we mean pseudo-sedimentary indicators including scouring and flow indicators, shearing of crystals or current bedding. Very little evidence for flow is found elsewhere, except at the contact with the marginal pegmatite and in Unit +3, which is associated with multiple roof rock autoliths (e.g. Fig. 2b).

The black kakortokite has a foliated texture and comprises 60% arfvedsonite, 20% alkali feldspar (which has a preferred alignment of crystal long axes, approximately parallel to the unit boundary), 15% eudialyte and 5% nepheline. The red kakortokite is saccharoidal in texture and comprises 40% eudialyte, 20% alkali feldspar, 20% nepheline, 10% arfvedsonite and 10% aegirine. The white kakortokite is typically foliated with the fabric identified by preferred alignment of alkali feldspar long axes approximately parallel to the unit boundary, although the fabric is less clearly visible than that in the black layer. It typically comprises 40% alkali feldspar, 20% nepheline, 10% sodalite, 10% arfvedsonite, 10% aegirine and 10% eudialyte. The white kakortokite of Unit 0 shows greater variation vertically through the layer. At the base, it is poikilitic with arfvedsonite oikocrysts, which enclose euhedral alkali feldspar and nepheline crystals; these oikocrysts decrease upwards and only occur in the lower 0.5 m of the unit. Sodalite, fluorite, aenigmatite and rinkite also occur within the kakortokites but are not analysed in the present study.

3. Crystal size distribution analysis

3.1. Development of igneous rocks — insights from CSDs

Textural analysis, through CSDs, has been applied within this study as a tool for understanding the processes through which magma solidified and equilibrated to produce the final rock texture, i.e. the geometric arrangement of crystals (cf. Higgins, 2006). CSD analysis provides insights into processes of nucleation and growth in igneous rocks (e.g. Cashman and Marsh, 1988; Higgins, 2006; Marsh, 1988, 1998) with plot shapes typically being attributed to specific processes. Log-linear slopes are associated with in situ crystallisation; slopes that curve upwards at large crystal sizes with gravitational settling; whereas slopes that curve downwards over the larger crystal sizes are inferred to form by crystal fractionation, i.e. the growth of crystals in suspension followed by enclosure in an upwards growing crystal pile (e.g. Marsh, 1988). However, a wide range of processes contribute to the development of igneous rocks and the effects of competing processes must be considered when interpreting CSD plots, as the final texture reflects a combination of kinetic, mechanic and equilibrium effects (Higgins, 2006).

Initial nucleation in a magma is driven by kinetics, associated with either undercooling or supersaturation of the system (Higgins, 2006). Two population models are cited within the development of igneous rocks: steady-state crystallisation and batch crystallisation (Higgins, 2006; Marsh, 1998). Steady-state crystallisation is rarely representative of geological systems, but is modelled to result in a linear relationship between population density and crystal size (Marsh, 1998), although changes in crystallisation parameters, e.g. residence time or nucleation density, can result in complexity within CSD plots at small crystal sizes (Higgins, 2006). Batch crystallisation applies CSD theory to growth within a closed system, thus is a better approximation of igneous systems (Higgins, 2006). Modelling of nucleation within this system results in log-linear CSDs that systematically migrate to larger crystal sizes with increasing crystallinity (Marsh, 1998). However, increasing crystallinity over 50% can result in curvature and slope complexity at the smallest crystal sizes (Higgins, 2006).

After nucleation and primary crystal growth, mechanical processes modify crystal populations through compaction, sorting and mixing. Mechanical compaction will affect the entire crystal population equally and has the effect of increasing the population density without modifying the CSD plot shape (Higgins, 2006). Importantly, pure mechanical compaction is not inferred to contribute to the development of foliation fabrics within the rocks (Higgins, 1991). Pressure-solution compaction can have a greater effect on the CSD plot shape as smaller crystals are preferentially dissolved, due to their greater surface energy to volume ratios, thus this process results in downwards-curvature of the CSD slope at small crystal sizes. Whilst this process has a similar effect on CSD patterns as coarsening, discussed below, the effects can be determined in the final rock textures through development of foliation (Higgins, 2006).

Sorting of crystals results from processes of crystal accumulation, which in this context is used to describe the process of separating crystals from magma via gravitational segregation, filter pressing, flow differentiation and/or crystallisation on conduit walls (Higgins, 2006). Accumulation is often considered to produce a CSD that curves upwards at larger crystal sizes (e.g. Marsh, 1988). However, the effects of this process via gravitational segregation on CSDs were modelled by Higgins (2002b) who found that the initial stages of accumulation (1% crystals) via gravity result in a log-linear CSD plot shape. With increasing crystal accumulation over time, the CSD plots retain their linear form, but rotate around the intercept. Minor curvature occurs as all crystals are precipitated, however this is reflected as a downturn at the smallest crystal sizes, importantly not as an upturn at the larger crystal sizes.

Mixing of crystal populations occurs as a result of magma mixing or mingling. The effects of this process can be observed via strong kinks in CSD plot shapes (e.g. Marsh, 1988), however mixing of two crystal populations with contrasting slopes and intercepts can produce a CSD with a steep slope at small crystal sizes, which lessens towards larger crystal sizes, i.e. has an upwards curvature due to the representation of two log-linear CSDs on a single plot (Higgins, 2006). Further complications to plot shapes occur following growth of the two crystal populations, as the growth of the existing crystals will displace the CSD towards larger crystal sizes, but should preserve log-linear segments of the mixed CSD plot shape (Higgins, 2006).

Equilibration is one of the most important processes to consider as this determines the final amount and size of crystals. A variety of terms are used to describe processes of equilibration, including Ostwald ripening, textural maturation, crystal ageing and annealing (cf. Higgins, 2011). However, all these terms can be considered under the general bracket of textural coarsening. As the kinetic driving forces (either undercooling or supersaturation) decrease, reducing the nucleation rate to zero, the system equilibrates through textural coarsening to minimise the total energy of the crystal population (Higgins, 2006). This occurs through crystal growth as larger crystals are more stable, due to a lower surface area to volume ratio, than smaller crystals (Higgins, 2006). Initial stages of growth occur at grain boundaries and are observed through modification of dihedral angles from original impingement textures to either solid-state equilibrium textures, with high median dihedral angles, or melt-mediated equilibrium textures with low median dihedral angles, when a single phase system is considered (Holness et al., 2005). Whilst several models for textural coarsening have been proposed, the most applicable to geological systems is the communicating neighbours (CN) model (DeHoff, 1991; Higgins, 1998), which implies that growth rates are not only dependent on crystal size, but are also affected by individual crystal characteristics and the position of the crystal with respect to its neighbouring crystals (Higgins, 2006, 2011). Combining this model of crystal growth with temperature cycling in the magma chamber (e.g. Simakin and Bindeman, 2008) indicates that temperature cycles of only a few degrees can result in macroscopic coarsening and produce CSDs similar to those observed in natural systems (Higgins, 2011). The effect of this process on CSD plots is observed through a downturn at the smallest crystal sizes, with fanning of the CSD slopes at larger crystal sizes (Higgins, 2006, 2011).

Multiple processes develop the various CSD plot shapes and the competing and/or overprinting effects of kinetic, mechanic and equilibration processes must be considered when interpreting CSD data in the context of determining primary processes of rock development.

3.2. CSD method

CSD analysis provides a measure of the number of crystals of a mineral per unit volume, within a series of defined size intervals (Marsh, 1988). Analysis of igneous rocks and, in particular, inferences about the effects of crystal settling were pioneered with studies of low viscosity basalts (Cashman and Marsh, 1988; Marsh, 1988). Given the low viscosity of agpaitic magmas (cf. Larsen and Sørensen, 1987), similar inferences can be made from the CSDs of these magma compositions.

This study calculates CSDs from thin sections via hand-digitised images following Higgins (2000), using CSDCorrections v. 1.4.0.2 (http://www.uqac.ca/mhiggins/csdcorrections.html). The data are plotted as population density (logarithmic number of crystals per unit volume) against crystal size intervals (maximum length) and plot profiles are interpreted following the theory described in Section 3.1 with reference to Higgins (1999, his Fig. 8) and Marsh (1988, his Fig. 7). The characteristic minerals from each layer (arfvedsonite in black; eudialyte in red; and alkali feldspar with nepheline in white kakortokites) are investigated. The other cumulus phases in the kakortokites (aegirine, sodalite, fluorite and aenigmatite) form a small proportion of each unit, thus analysis would not provide statistically reliable insights into unit development. Only the characteristic minerals for each layer (i.e. arfvedsonite in black kakortokite, eudialyte in red and alkali feldspar and nepheline in the white kakortokite) were used as they form the bulk of the rock and the high percentages of each mineral (up to 60 mod.%) allow for a rigorous quantitative textural analysis. Thus, the data are chosen to optimise insights into the processes that contributed to the formation of the layers. To negate the effects of late-stage alteration, which particularly affects eudialyte and nepheline, relict eudialyte was only included where the original crystal outlines were preserved and could be confidently identified as pseudomorphs (Fig. 3a). Nepheline was excluded where altered, as the original crystal outlines were not preserved, thus nepheline data are not presented for all white kakortokites. Any minerals interpreted as intercumulus, i.e. anhedral crystal shapes and/or interstitial textures, were also excluded from the CSD analysis, as these do not provide insights into the primary processes of layer formation and development.

Aspect ratios used for each mineral are based on crystal habits with reference to the CSDSlice database (Morgan and Jerram, 2006): 1:1.4:2.8 for arfvedsonite, 1:1.15:1.5 for eudialyte, 1:3.2:5.5 for alkali feldspar and 1:1.15:1.6 for nepheline. Any crystal alignment was determined through CSDCorrections and input to calculate CSD profiles. The smallest grain-size reported is inferred to be the lower limit of a sample as the smallest crystals of each studied mineral are easily visible (cross-checked with BSE images). Accordingly, all grains in the sample were measured with the use of circularly polarised light (CPL). Use of CPL ensures that all minerals display their greatest birefringence and thus enhances the visibility of low birefringence minerals such as nepheline and feldspars (Higgins, 2010).

3.3. CSD results

CSD data are presented in Fig. 4; the supplementary files contain the input and output data (Table SF1) and the raw data (Table SF2). Each dataset, excluding the alkali feldspar plots, has a central region with a negative slope that visually approximates to a log-linear relationship (Fig. 4), although some plots show minor curvature. The behaviour of smaller crystal populations is variable; some project along the central trend (Fig. 4i), others swerve up (Fig. 4c) or down (Fig. 4g). The populations of larger crystals sometimes extend the central region (Fig. 4g) but in other cases flatten (Fig. 4e). Whilst the central regions of the graphs are consistent, the behaviour of smaller and larger crystal populations is not a function of the mineral type, and even varies between different localities for the same mineral in the same unit (Fig. 4h). These trends do not comply with one simple process of crystal formation, but indicate multiple competing crystal growth mechanisms.

The Unit −1 white kakortokite CSDs have log-linear central regions for both the alkali feldspar (R-squared coefficient of 0.99) and nepheline (R-squared coefficient of 1.00), with downturns at the smallest crystal sizes (Fig. 4a–b). The alkali feldspar crystal sizes determined from CSDCorrections range from 1.5 to 9.7 mm, and the CSD slope value calculated from linear regression of the central region of the CSD is $-0.62\ mm^{-1}$. The nepheline crystal sizes range from 0.6 to 2.3 mm and the slope value is $-1.23\ mm^{-1}$.

The CSDs for Unit −1 white kakortokite sampled immediately below (0–25 mm) the Unit −1/Unit 0 boundary (Fig. 1) have a range of plot shapes (Fig. 4c–d). The alkali feldspar CSDs for samples from Locations A to B are kinked with an R-squared coefficient between 0.97 and 0.98, whereas Locations C and D are relatively log-linear with R-squared coefficients from 0.99 to 1.00. Additionally, Locations A to C have upward kinks at the smallest crystal sizes, representing an increased population density, whereas Location D indicates a downturn instead (Fig. 4c). Nepheline was only analysed at Location C and the CSD has a flattening at the smallest crystal sizes (Fig. 4d), it has a log-linear plot shape with an R-squared coefficient of 1.00. The alkali feldspar crystal sizes range from 0.01 to 11.3 mm and the CSD slope values for the relatively log-linear central regions range from -0.68 to $-0.81\ mm^{-1}$ with R-squared coefficients of 0.97–1.00. The nepheline crystal sizes range from 0.4 to 2.3 mm and the CSD slope value, excluding the flattened region, is $-3.00\ mm^{-1}$.

The arfvedsonite CSDs for the samples immediately above (0–25 mm) the Unit −1/Unit 0 boundary (Fig. 1) have similar slope profiles to the arfvedsonite CSDs from the central regions (Fig. 1) of the Unit 0 black kakortokite (Fig. 4e–f). The arfvedsonite crystal sizes range from 0.1 to 5.0 mm immediately above the boundary and between 0.2 and 5.0 mm in the centre of black layers. All CSDs, except U-1/0 Location C and U0 Location B, have kinks at larger crystal sizes: Locations A (boundary), A (layer), B (boundary) and D (boundary) show kinked plots at 3.18 mm (Fig. 4e), 3.17 mm (Fig. 4f), 1.27 mm (Fig. 4e) and 2.02 mm (Fig. 4e), respectively. The CSD plots for the boundary samples have slopes that curve upwards at the largest crystal sizes (R-squared coefficients between 0.83 and 0.98). The central portion of the Unit 0 black kakortokite shows a slope that curves upwards at large crystal sizes (R-squared coefficient of 0.97) at Location A and a log-linear slope (R-squared coefficient of 1.00) at Location B. The slope values for all CSDs range from -3.73 to $-5.15\ mm^{-1}$.

The CSDs for the eudialyte in the red kakortokite samples (Fig. 4g) are log-linear with R-squared coefficients between 0.98 and 1.00. The crystal sizes range from 0.4 to 2.3 mm and the slope values for the central regions range from -4.26 to $-5.20\ mm^{-1}$.

The Unit 0 white kakortokite alkali feldspar CSDs have a range of slope patterns (Fig. 4h). Locations A to B have slopes that are concave-downwards over the range of crystal sizes (R-squared coefficient of 0.96 to 0.99) with downturns at the smallest crystal sizes. Location C has a slope that is log-linear with an R-squared coefficient of 0.99. Location D was sampled from the first 0.5 m of the Unit 0 white kakortokite (Fig. 1) and displays the oikocrystic texture. Large (up to 12 mm) arfvedsonite oikocrysts host euhedral crystals of nepheline and alkali feldspar (Fig. SF2h). The CSD plot has a convex-upwards slope over the entire range of crystal sizes (R-squared coefficient of 0.94) and an increased population density at the smallest crystal sizes. Despite the range of patterns, the crystal sizes and CSD slope values are similar between locations. The crystal sizes range from 0.2 to 9.5 mm and the central regions of plots have slope values ranging between -0.61 and $-0.79\ mm^{-1}$ (Table SF1). The nepheline data from the Unit 0 white kakortokite have log-linear slopes (R-squared coefficients of 0.99–1.00). The crystal sizes vary between 0.2 and 3.5 mm and the slope values for the central regions range from -2.04 to $3.87\ mm^{-1}$.

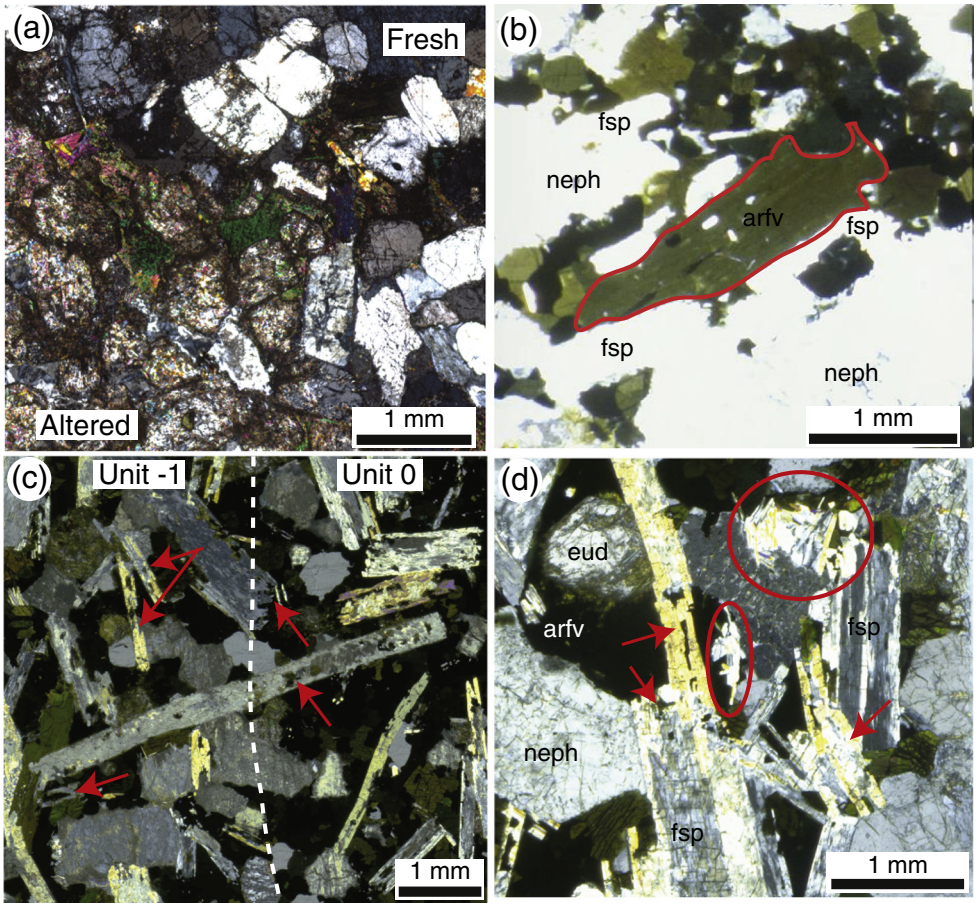

Fig. 3. (a) Alteration of eudialyte (lower) develops a poly-crystalline (multi-coloured) texture within high relief outlines of relict euhedral eudialyte, from Unit 0 red kakortokite, Location B. (b) Arfvedsonite phenocryst (outlined) surrounded by groundmass of arfvedsonite, nepheline and alkali feldspar in Unit 0 black kakortokite, Location A. (c) Unit −1/Unit 0 boundary (dashed line) from Location C. Embayed alkali feldspar crystals are indicated by arrows. (d) Clots of microcrystic alkali feldspar (encircled) in Unit −1 white kakortokite (Location A) 20 mm below the Unit −1/Unit 0 boundary. Embayed alkali feldspar crystals are marked by arrows. NB all rock sections are photographed under circularly polarised light. Arfvedsonite can appear opaque in thick section. Abbreviations: arfv — arfvedsonite; eud — eudialyte; fsp — alkali feldspar; neph — nepheline.

CSD data were verified through comparing the phase percent calculated from the total area of the crystals and the CSD itself (c.f. Higgins, 2002a) applying equations for both linear and curved CSDs where appropriate. The data are consistent, thus the CSDs are inferred to have been correctly determined from 2 dimensional measurements. A plot of slope vs. Lmax (mean size of the 4 largest crystals) shows a positive correlation between the arfvedsonite, eudialyte and nepheline data, whereas the alkali feldspar data plot in a separate grouping (Fig. 5a). A plot of volumetric phase abundance vs. characteristic length (−1/slope) displays a grouping of the arfvedsonite and eudialyte data, whereas the nepheline and alkali feldspar data are more variable (Fig. 5b).

4. Eudialyte chemistry

4.1. EPMA method

Backscattered electron (BSE) imaging and electron probe microanalysis (EPMA) of targeted eudialyte crystals were performed at the University of St Andrews using the JEOL JXA-8600 superprobe in wavelength dispersion mode. Compositions were obtained using the operating conditions of Pfaff et al. (2008): an acceleration voltage of 20 kV, a beam current of 20 nA and a defocused beam of 10 μm diameter to measure all elements. Count-times on peaks for major elements were 16 s and 30–120 s for minor elements. Background measurement times were half of the peak times. Na was measured first with a count time of 10 s on peak and 5 s on background to avoid atom migration from the analysed spot. A combination of natural and synthetic standards was used and corrections were internally performed using PAP (Armstrong, 1991).

The term *eudialyte* is used throughout for the *eudialyte-group minerals* (EGM, Johnsen et al., 2003). Their formulae were calculated through normalisation of the sum of the Si + Zr + Ti + Nb + Al + Hf cations to 29 a.p.f.u (Johnsen and Grice, 1999). End-member eudialyte compositions were determined following the methodology of Pfaff et al. (2010).

4.2. EPMA results

The eudialyte chemical data are presented in Figs. 6–7, the investigated elemental ratios in Table 2 and the raw data files are located in the supplementary materials, Table SF3.

Compositions of the EGM range between eudialyte (*s.s.*), kentbrooksite and ferrokentbrooksite (Fig. 6). Eudialyte crystals from each rock type plot in a distinct grouping, from relatively Mn-poor compositions in black kakortokite to relatively Mn-rich compositions in white kakortokite. Analysing this using the $Fe_{(TOT)}$/Mn ratio (Pfaff et al., 2008; Schilling et al., 2011) further illustrates this variation in composition (Fig. 7a–b, Table 2). The eudialyte in the black kakortokite has the greatest $Fe_{(TOT)}$/Mn ratios, between 10.85 and 13.34. The eudialyte in red kakortokite ranges from 7.23 to 10.55 and eudialyte in white kakortokite has the lowest $Fe_{(TOT)}$/Mn ratios between 5.77 and 9.98. Eudialyte from white kakortokite immediately below the boundary (0–25 mm) has similar $Fe_{(TOT)}$/Mn ratios (4.76–9.45) to those from the Unit −1 white kakortokite (6.62–9.50). There is a

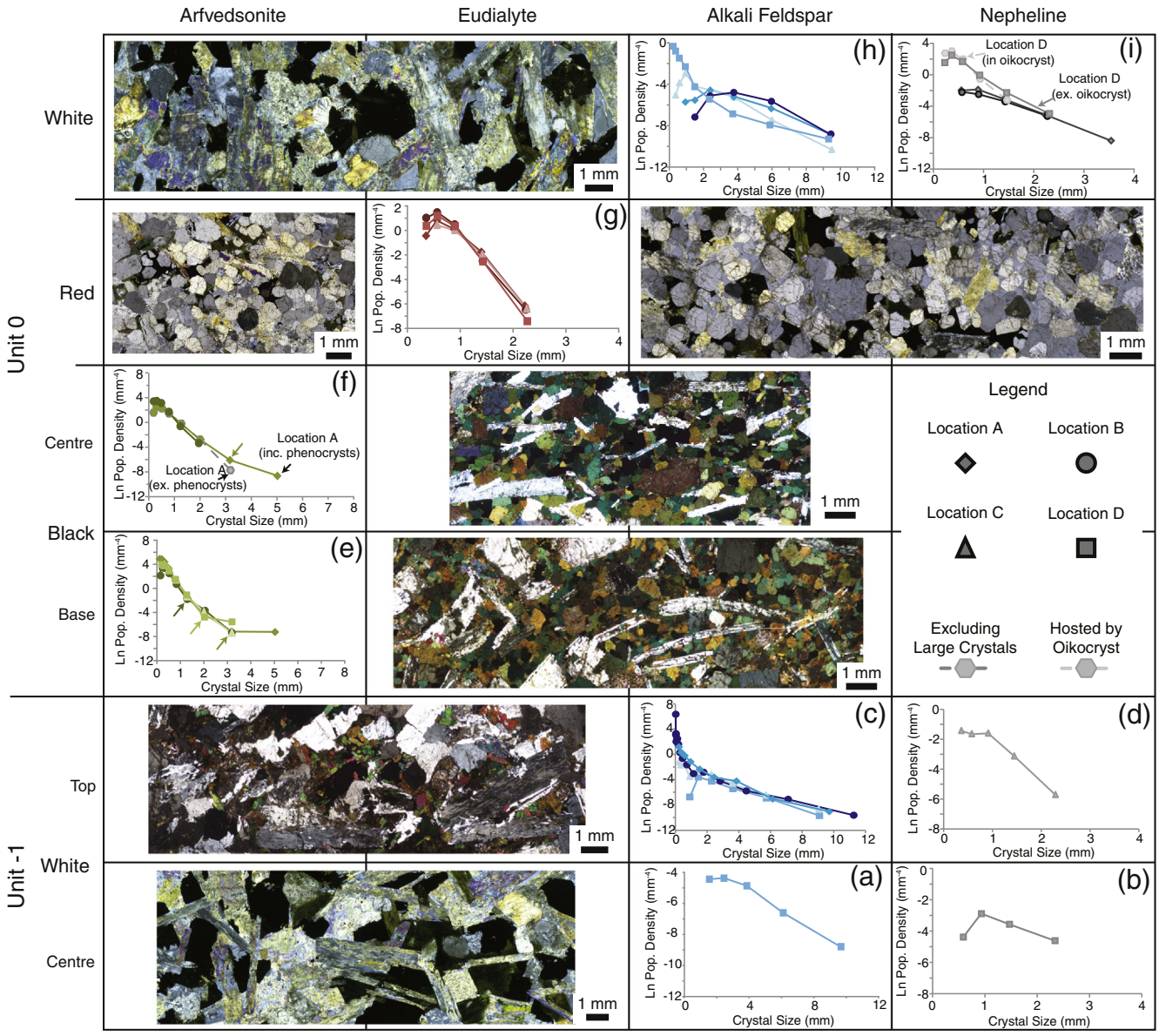

Fig. 4. CSD plots and photomicrographs of representative samples arranged according to mineralogy and stratigraphy. All input and output data are located in Table SF1. (a) Unit −1 alkali feldspar in white kakortokite at Location D. (b) Unit −1 nepheline in white kakortokite at Location D. (c) Alkali feldspar immediately below the Unit −1/Unit 0 boundary in Unit −1 white kakortokite. (d) Nepheline immediately below the Unit −1/Unit 0 boundary in Unit −1 white kakortokite. (e) Arfvedsonite immediately above the Unit −1/Unit 0 boundary in Unit 0 black kakortokite. (f) Unit 0 arfvedsonite in black kakortokite. (g) Unit 0 eudialyte in red kakortokite. (h) Unit 0 alkali feldspar in white kakortokite. (i) Unit 0 nepheline in white kakortokite. Photomicrographs: U-1 white centre = EJH/12/081, U-1 white top = AF/99/195, U0 black base = AF/99/195, U0 black centre = AF/99/192, U0 red = EJH/12/007 (left) and EJH/12/080 (right), U0 white = EJH/12/010. NB scales vary to optimise the visibility of each plot. Samples near Unit −1/Unit 0 boundary are 0–25 mm above/below the unit boundary.

discontinuity across the Unit −1/Unit 0 boundary as the eudialyte crystals from the Unit 0 black kakortokite immediately above the boundary (0–25 mm) have a larger range of, and reduced, ratios (7.95–13.18) compared to those in the central regions of the Unit 0 black kakortokite layer (10.85–13.34).

The range of Ca/(REE + Y) ratios exhibits little variation within error through the Unit −1/Unit 0 boundary and Unit 0 (Fig. 7c–d, Table 2). There is a general trend of decreasing values upwards through Unit 0 and a small change in values occurs across the Unit −1/Unit 0 boundary. The outlying low values are associated with eudialyte crystals that were shown by petrographic analysis to be partially pseudomorphed (e.g. Borst et al., 2016). There is a general decrease in Cl content of the eudialyte crystals upwards through Unit 0 (Fig. 7e–f, Table 2). There is a discontinuity in Cl content at the Unit −1/Unit 0 boundary as the eudialyte crystals in the U-1 white kakortokite have lower Cl contents than those in the overlying black kakortokite of U0. Eudialyte crystals in the Unit 0 white kakortokite have the greatest variation between locations.

5. Discussion

5.1. Formation of Unit 0

The CSD slopes of the present study (Fig. 4) show a range of plot profiles, which fall into several common themes. All of the profiles are broadly log-linear but with modification at the small and large crystal regions reflecting a range of modifying influences. The details of each profile are given below.

CSD plots from the black kakortokites at base of Unit 0 (0–25 mm above the unit boundary, Fig. 1) have different plot shapes (Fig. 4e) compared to the plots from the central portion of the black layer (~0.5 m above the unit boundary, Figs. 1 & 4f). The CSD plots for the

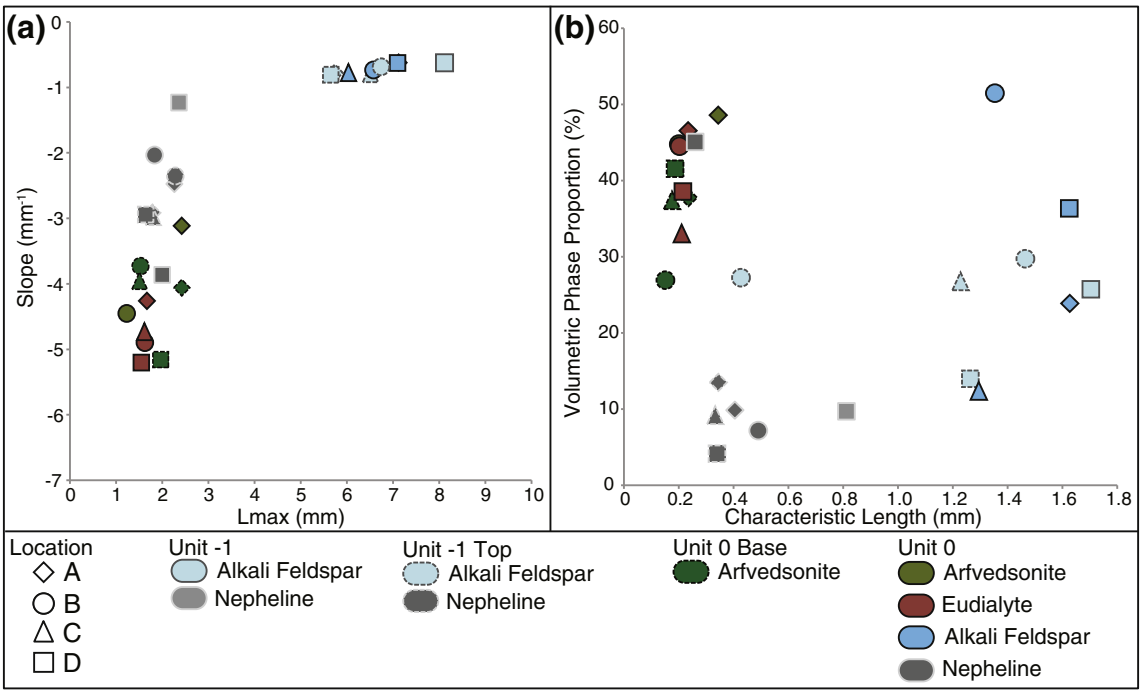

Fig. 5. (a) Plot of slope vs. Lmax indicating positive correlation between arfvedsonite, eudialyte and nepheline data. Alkali feldspar data plot in separate grouping. (b) Plot of volumetric phase proportion vs. characteristic length highlighting the variability in the dataset. NB in all plots error bars are smaller than symbols.

samples near the boundary display marked kinks (arrowed, Fig. 4e), whereas the plots for the central portion of the layer are curved (Location A) or log-linear (Location B, Fig. 4f). Kinked plots represent mixed crystal populations (e.g. Marsh, 1988), but this can also result from a variety of processes. The CSD plot for Location A in the central portion of the layer provides more insight into those processes. This sample contains some large arfvedsonite crystals, which are euhedral and markedly larger than the groundmass (Fig. 3b), similar to the samples from the

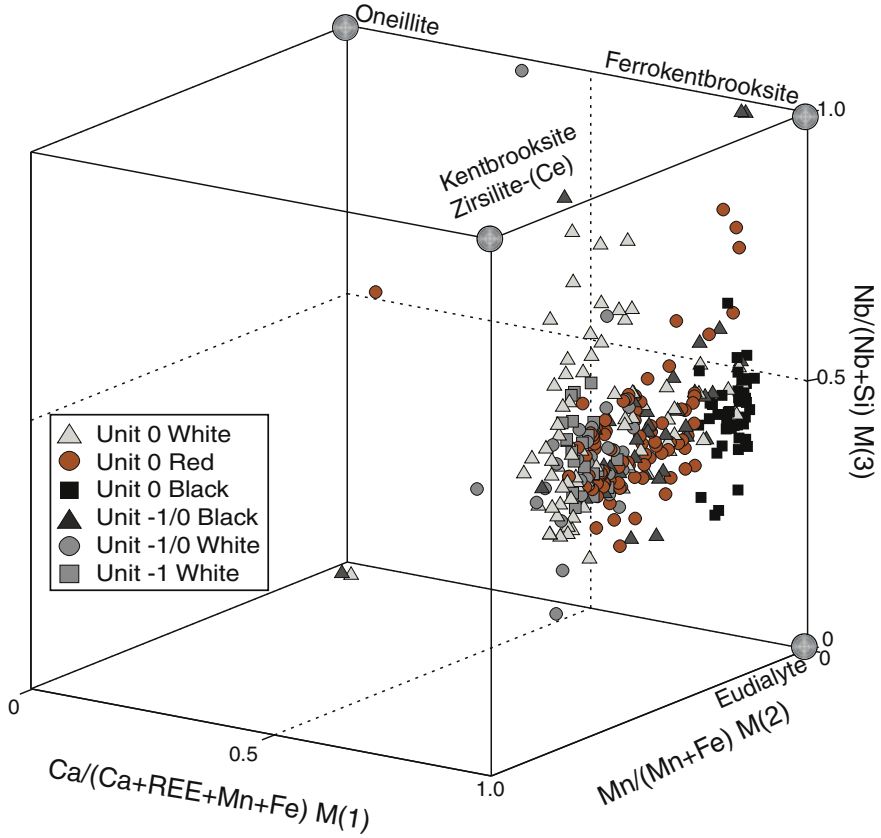

Fig. 6. 3D scatterplot of Ca/(Ca + REE + Mn + Fe) on the M(1) site vs. Mn/(Mn + Fe) on the M(2) site vs. Nb(Nb + Si) on the M(3) site. End member compositions plotted from Sjöqvist et al. (2013).

unit boundary. When these large crystals are excluded from the analysis, the resultant CSD is log-linear (R-squared coefficient of 0.99, Fig. 4f) and indicative of formation of the groundmass arfvedsonite through kinetically controlled nucleation and growth, which is inferred to occur in situ at the interface between the crystal mush and the magma. The concave upwards curvature of the CSD plot for the entire sample (Fig. 4f) is interpreted as the effects of mixing two crystal populations, i.e. the groundmass, which developed in situ, and the larger crystals. Due to the presence of larger crystals, accumulation processes, i.e. gravitational settling into the basal layer from the magma above, cannot be excluded from the development of the black kakortokite layer.

The CSDs for red kakortokite samples (Fig. 4g) are log-linear, indicating the bulk of the eudialyte formed through kinetically controlled nucleation and growth, inferred to be associated with in situ crystallisation. The minor curvature in some plots however, indicates that in situ crystallisation was accompanied by processes of density segregation with some crystals remaining in suspension, i.e. Marsh's (1988) fractional crystallisation, but this was a minor contributor to layer development.

The white kakortokite samples have a range of CSD patterns (Fig. 4h, i) that vary between localities and with stratigraphic height (Fig. 1). This range of patterns is inferred to be associated with processes of accumulation following kinetically controlled nucleation and growth of crystals throughout the magma body. The lower portion of white kakortokite is characterised by CSD plots that have an upwards curvature over the larger crystal sizes. This is inferred to be associated with gravitational segregation and settling of alkali feldspar during development of the lower portion of the white layer. The CSD plots for samples from the upper portion of the white layer show curvature (concave-downwards) over the entire range of crystal sizes, which is also consistent with accumulation processes, but with alkali feldspar crystals remaining in suspension in the magma. Thus, processes of accumulation and gravitational settling were contributors to forming the white kakortokite layer. It should however be noted that the large alkali feldspar crystal sizes resulted in a reduced number of crystals within the section, thus fewer crystals were analysed. Therefore these interpretations are based on populations of <200 crystals (Table SF2), below the minimum indicated for statistically reliable analysis (Mock and Jerram, 2005), thus the slope patterns may not be a reliable indicator of the processes involved in the development of white kakortokite. The nepheline plots (Fig. 4i), however, are more consistent with the bulk of the nepheline crystals forming through kinetically controlled in situ crystallisation at the crystal mush–magma interface.

Further analysis of the CSD data through slope and Lmax (Fig. 5a) indicates nucleation through a batch crystallisation model with a constant nucleation rate and, except the alkali feldspar, an effective growth rate that increases exponentially with crystal size (Marsh, 1998). The alkali feldspar data indicate a constant growth rate (Marsh, 1998).

5.2. Textural development of Unit 0

The kakortokites are often associated with a fabric defined by preferred orientations of the acicular or tabular minerals (arfvedsonite and alkali feldspar). There are three common methods through which a preferred orientation can develop within magmatic cumulates (cf. Meurer and Boudreau, 1998). A foliation fabric, without lineations, can be developed through settling of crystals in quiescent conditions (Brothers, 1964; Meurer and Boudreau, 1998), as during settling particles will become orientated with their principal cross-sectional area perpendicular to the direction of motion (McNown and Malaika, 1950). Deposition in strong flow regimes can also produce a preferred orientation of crystals, due to shear stress, and lineations typically also develop (Meurer and Boudreau, 1998). Compaction through processes of pressure-solution can produce a foliation fabric, typically with lineations, and can be distinguished by recrystallisation and deformation of crystals (Meurer and Boudreau, 1998). As the fabric in the kakortokites is marked by the preferred orientation of crystals without the development of lineations or deformation of crystals, it is unlikely to have formed purely through pressure-solution associated with compaction. However, the alignment of alkali feldspar crystals is stronger in the black kakortokites than in the white, thus compaction is inferred to have contributed to the development of the fabric (e.g. Upton, 1961). The lack of flow indicators throughout the units also indicates that development of the fabric through shear stress associated with magmatic flow is unlikely. Further, alkali feldspar crystals with long aspect ratios lie across the Unit −1/Unit 0 boundary (Fig. 3c) and these are unlikely to have been preserved during magmatic flow. The fabrics throughout the black, red and white layers within Unit 0 are always associated with preferred alignment of alkali feldspar only. Other units may also have a fabric in the red and white kakortokites that is further defined by acicular arfvedsonite crystals. These subordinate phases were not investigated through CSD analysis due to the limited number of crystals within a section, thus accumulation of these crystals through gravitational settling cannot be discounted and indeed the CSDs indicate that alkali feldspar in the white kakortokites did accumulate through gravitational segregation. Therefore, the fabric is inferred to have primarily developed through sedimentation within a quiescent magma, but enhanced by late stage compaction as the cumulate pile grew during development of the layered kakortokite series and overlying rocks.

The final process modifying the textures of the kakortokites is equilibration. The samples in this study exhibit textural features of coarsening including modification of apparent dihedral angles and increased curvature of crystal faces (e.g. Higgins, 2011). Most of the CSD plots have a downturn at the smallest crystal sizes, and, although this feature can be accounted for by a range of processes (see Section 3.1), the petrographic indicators of coarsening reflect final modification of textures and CSD patterns through equilibration. This is inferred to have occurred through the CN (communicating neighbours) model rather than purely through a process such as Ostwald ripening, which only accounts for micron-scale processes of crystal growth and dissolution (Cabane et al., 2005).

This later-stage process of grain growth is inferred to have occurred by grain-overgrowth, while the kakortokite layers were still in a 'mushy' state. This would have modified the CSD profiles, complicating the interpretation of the slope patterns. From this and the CSD slopes, processes of gravitational settling cannot be discounted from contributing to the development of Unit 0. However, we infer that processes of in situ crystallisation played the dominant role in the development of at least the black and red kakortokites of Unit 0.

5.3. Hypotheses for development of layering

5.3.1. Density segregation

The subdivision of the kakortokite units into black, red and white layers is consistent with 'normal' density layering, i.e. the densest phase, arfvedsonite, is concentrated at the base of the unit, whereas the less dense phases, alkali feldspar and nepheline, are concentrated in the upper portions of the unit. This density grading led many authors to attribute the tripartite nature of the layering to density segregation of coevally nucleating and growing phases during gravitational settling (e.g. Bohse et al., 1971; Ferguson, 1964; Larsen and Sørensen, 1987; Ussing, 1912). This theory is extended, at least during the development of the lowest exposed kakortokite units, to infer that sodalite was also a cumulus crystallising phase, which due to its low density, floated in the magma and formed the naujaite as a flotation cumulate at the roof of the chamber (e.g. Sørensen, 1969; Ussing, 1912). This provides an elegant and simple explanation for the tripartite nature of the layering, but does not correlate with the textural data above, nor account for the repetition of the layering, as 29 units occur within the kakortokite outcrops. Thus, simple density sorting is untenable.

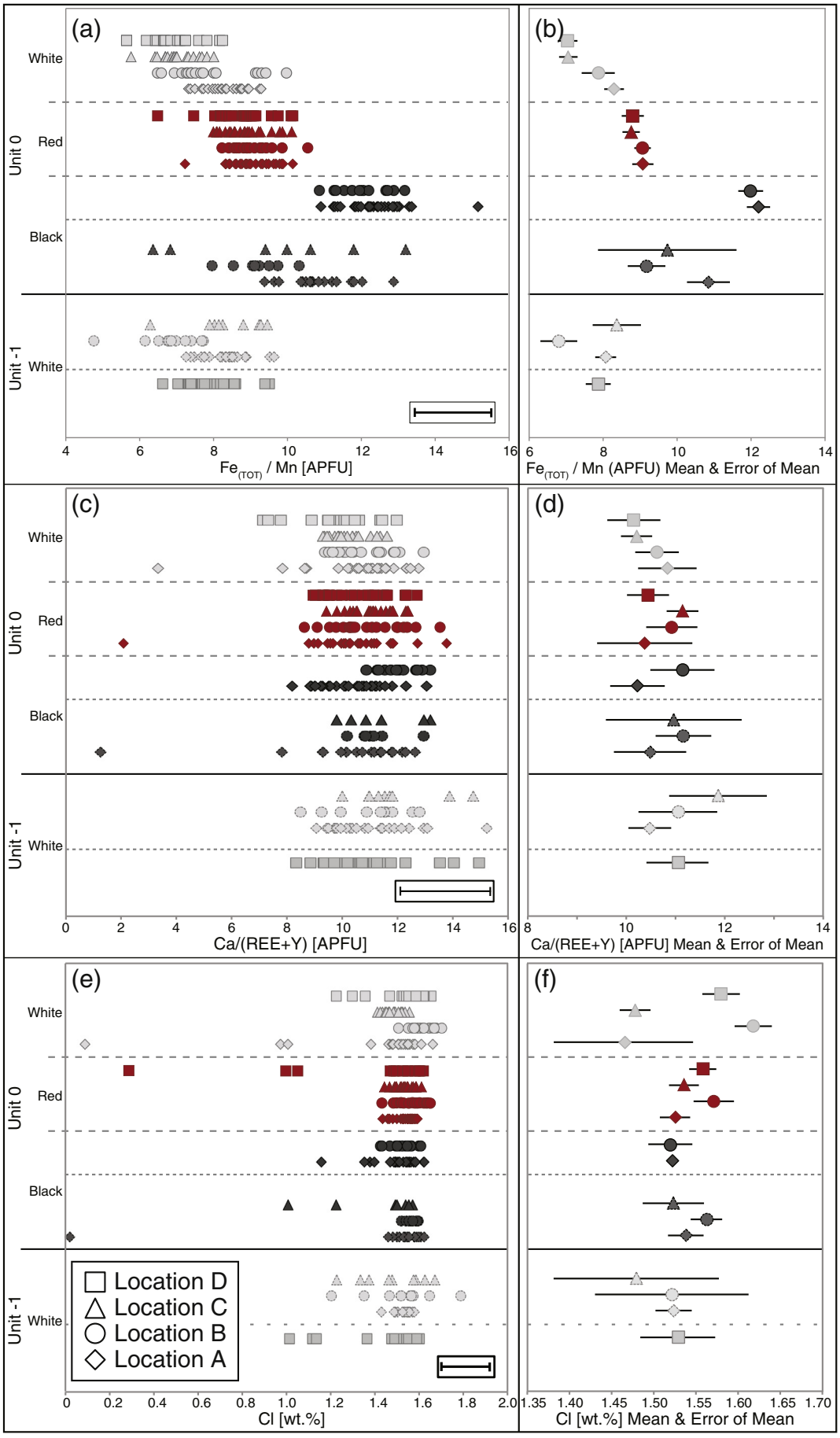
(a)
(b)
(c)
(d)
(e)
(f)
White
Red
Black
Unit 0
Unit -1
Fe(TOT) / Mn [APFU]
Fe(TOT) / Mn (APFU) Mean & Error of Mean
Ca/(REE+Y) [APFU]
Ca/(REE+Y) [APFU] Mean & Error of Mean
Cl [wt.%]
Cl [wt.%] Mean & Error of Mean
Location D
Location C
Location B
Location A

Table 2
Range of $Fe_{(TOT)}$/Mn, Ca/(REE + Y) ratios and Cl wt.% values in eudialyte crystals according to rock type and sample location. Precision (±) reported to 95% confidence.

Unit	Rock		$Fe_{(TOT)}$/Mn				Ca/(REE + Y)				Cl (wt.%)			
			Mean	±	Min	Max	Mean	±	Min	Max	Mean	±	Min	Max
U-1	White	D	7.87	0.34	6.62	9.50	11.04	0.63	8.83	14.92	1.53	0.04	1.13	1.60
U-1/0 Boundary	White	Mean	7.73	0.35	4.76	9.45	11.05	0.45	8.48	14.71	1.51	0.04	1.20	1.79
		A	8.07	0.28	7.25	8.85	10.48	0.43	9.49	11.68	1.52	0.02	1.43	1.58
		B	6.80	0.50	4.76	7.72	11.05	0.80	8.48	12.77	1.52	0.09	1.20	1.79
		C	8.37	0.65	6.29	9.45	11.86	0.99	9.99	14.71	1.48	0.10	1.23	1.67
	Black	Mean	10.33	0.54	7.95	13.18	10.79	0.47	7.81	12.93	1.54	0.01	1.48	1.60
		A	10.85	0.58	9.37	12.86	10.48	0.73	7.81	12.15	1.54	0.02	1.48	1.60
		B	9.17	0.51	7.95	10.31	11.16	0.56	10.16	12.92	1.56	0.02	1.52	1.59
		C	11.08	1.73	9.40	13.18	10.96	1.38	9.79	12.93	1.52	0.04	1.49	1.57
U 0	Black	Mean	12.10	0.23	10.85	13.34	10.67	0.45	8.85	14.32	1.52	0.02	1.35	1.62
		A	12.20	0.31	10.89	13.34	10.23	0.55	8.87	13.03	1.52	0.03	1.35	1.62
		B	11.99	0.34	10.85	13.16	11.14	0.65	8.85	14.32	1.52	0.03	1.42	1.61
	Red	Mean	8.93	0.13	7.23	10.55	10.72	0.31	2.09	13.78	1.55	0.01	1.43	1.65
		A	9.07	0.29	7.23	10.14	10.37	0.97	2.09	13.78	1.52	0.02	1.44	1.59
		B	9.07	0.22	8.23	10.55	10.92	0.52	8.63	13.54	1.57	0.02	1.43	1.65
		C	8.76	0.23	7.99	9.87	11.14	0.32	9.44	12.38	1.54	0.02	1.44	1.61
		D	8.80	0.30	7.46	10.15	10.44	0.43	8.96	12.32	1.56	0.02	1.49	1.61
	White	Mean	7.59	0.20	5.77	9.98	10.47	0.24	7.31	12.92	1.53	0.03	0.97	1.70
		A	8.30	0.27	7.33	9.30	10.83	0.59	7.83	12.74	1.47	0.08	0.97	1.66
		B	7.87	0.45	6.49	9.98	10.62	0.44	9.36	12.92	1.62	0.02	1.50	1.70
		C	7.06	0.25	5.77	8.01	10.21	0.32	9.29	11.60	1.48	0.02	1.41	1.55
		D	7.04	0.27	6.20	8.26	10.15	0.54	7.31	11.95	1.58	0.02	1.46	1.65

5.3.2. Crystal mats

It has been hypothesised that the layering developed through the formation of 'crystal mats' (Bons et al., 2015; Lindhuber et al., 2015; Marks and Markl, 2015). This hypothesis explains the regularity of the repetitive macrorhythmic layering, but does not account for the modes of development inferred in the present study. The 'crystal mats' hypothesis has three main requirements: the magma must not be convecting (Lauder, 1964); the density of the magma must be such that arfvedsonite will settle, whereas alkali feldspar is buoyant (Lindhuber et al., 2015); and the crystals can sink or float a significant distance, although not necessarily the entire height of the magma chamber, before they become trapped (Bons et al., 2015). In such models, the processes of gravitational settling and fractionation are key. Nucleation of each of the main minerals (arfvedsonite, eudialyte and alkali feldspar) is contemporaneous (Lindhuber et al., 2015) and the layering is formed due to interference between the coupled processes of settling and rising crystals (Bons et al., 2015). This caused the densest phase (arfvedsonite) to become trapped at certain horizons and the acicular shape of the arfvedsonite crystals contributed to the development of cohesive mats (Lindhuber et al., 2015). This, however, does not correlate with the CSD data, which indicate that the bulk of the arfvedsonite crystals forming the black kakortokite developed in situ, rather than accumulating through gravitational settling. However, although Lindhuber et al. (2015) illustrated the formation of mats in terms of crystal settling and rising, the development of arfvedsonite mats through in situ crystallisation cannot be discounted. These 'crystal mats' would result in the development of magma layers, which are semi-isolated from the resident magma and act as barriers to settling/flotation (Bons et al., 2015). Each unit is inferred by Lindhuber et al. (2015) to have formed quasi-independently as a crystallisation cell composed of an arfvedsonite-rich mat with an overlying magma-rich crystal mush. Bons et al. (2015) on the other hand, infer that buoyant alkali feldspar crystals became trapped underneath a 'mat', contributing to the formation of white kakortokite layers, with or without a horizon of melt lying between the buoyant layer and the underlying mat. Importantly for the understanding of kakortokite development, the two models differ on the permeability of the 'crystal mats'. Bons et al. (2015) infer that the mats would be porous enough to allow for the migration of melt during late-stage equilibration and/or compaction. Lindhuber et al. (2015) and Marks and Markl (2015) instead apply textural observations to infer that alignment of arfvedsonite crystals would make the 'mats' impermeable to both crystals and melt. The petrography and textures associated with the Unit −1/Unit 0 boundary investigated in the present study do not corroborate this, as they instead indicate infiltration of melt to some extent below the unit boundary (discussed fully below), which are inconsistent with impermeable mats (Lindhuber et al., 2015; Marks and Markl, 2015).

Whilst the 'crystal mat' hypothesis explains the regularity of the layering, other lines of evidence are inconsistent with it. For example, the autolith within Unit +3 detached from the roof series (Steenfelt and Bohse, 1975) and compressed the underlying units, whereas the overlying units drape over the autolith (Fig. 2b). These field observations indicate that the kakortokite layers formed *sequentially* from the bottom up and that the topmost layer was open to the magma chamber. In models where layering is formed by interference between linked processes with different rates operating in different directions, whether that is chemical diffusion (e.g. Larsen and Sørensen, 1987) or the physical competition between sinking and rising crystals (Bons et al., 2015; Lindhuber et al., 2015), all form at the same time. In addition, there would have been long periods prior to complete solidification of the arfvedsonite mats, during which the density contrast between the mat and the underlying magma or feldspathic crystal mush would favour slumping of the arfvedsonite, in an analoque to soft sediment deformation. Our field studies show no evidence, even locally, for areas where the denser arfvedsonite has collapsed downwards. Furthermore, the mineral textures and chemistries reported by Lindhuber et al. (2015) and in the present study are inconsistent with the 'crystal mats' model alone. If the 'mats' resulted in the trapping of buoyant alkali feldspar crystals (Bons et al., 2015; Marks and Markl, 2015), then the top of each unit should resemble the naujaite, which is inferred to have formed as a flotation cumulate (e.g. Upton, 2013), with euhedral alkali feldspar crystals surrounded by oikocrysts of arfvedsonite and eudialyte. Alternatively, trapping of early formed euhedral eudialyte

Fig. 7. Eudialyte chemistry measured by EPMA, subdivided according to stratigraphy and sample location. (a) $Fe_{(TOT)}$/Mn ratios. (b) Mean and error of mean for $Fe_{(TOT)}$/Mn data. (c) Ca/(REE + Y). (d) Mean and error of mean for Ca/(REE + Y) data. (e) Cl wt.%. (f) Mean and error of mean for Cl data. Mean and error of mean calculated to 95% confidence for each dataset. Note outliers are not excluded from mean calculations.

crystals that remained in suspension, which the CSD data indicate is possible, should preserve relatively primitive compositions in these crystals, as they would be trapped during the early stages of unit crystallisation. However, no such textures are seen at the top of any of the units; the only oikocrystic textures are observed at the base of the white layers (Fig. SF2h). The units typically have sharp basal contacts, which is accommodated by the 'crystal mat' models, but the gradational contacts between layers within units are hard to reconcile with simple density sorting during gravitational settling. Additionally the eudialyte compositional data presented above (Section 4) and in previous studies (Lindhuber et al., 2015; Marks and Markl, 2015; Pfaff et al., 2008) do not indicate relatively primitive eudialyte crystals to be present at the top of any of the units. Instead the eudialyte crystals in Unit 0 are marked by a continuous evolutionary profile (discussed fully below).

The inconsistencies between CSD, textural and compositional data and the 'crystal mats' model indicate that a different model must be considered for the origin of the layering in the kakortokites.

5.3.3. Sequential change in volatile content

Larsen and Sørensen (1987) proposed that the repetition of the layering resulted from a compositionally stratified magma chamber. Heat loss through the roof rocks developed a temperature gradient through the magma chamber, which resulted in the formation of concentration gradients and compositional stratification. Each unit is inferred to have developed due to loss of volatiles upwards, with the nucleation order being controlled by volatile element concentrations and degree of undercooling. High concentrations of volatile elements are suggested to supress nucleation within the magma body, except in a basal layer, which lost heat and volatile elements to the overlying layer. This allowed for nucleation and growth of minerals, initially arfvedsonite and eudialyte then alkali feldspar and nepheline with density segregation during gravitational settling enhancing the layering. A similar model was invoked by Bailey et al. (2006) for development of microrhythmic layering in the arfvedsonite lujavrite. They advocate crystallisation in a stagnant basal layer with alternate crystallisation of a dark layer (arfvedsonite-, nepheline-, sodalite- and microcline-rich) and a light urtite layer (sodalite-free and microcline-poor) controlled by variations in volatile concentrations and activities.

5.4. Model for formation of Unit 0

A sequential change in volatile content and in particular the concentration of halogens is the preferred cause of the repetition of the layering. We adopt a modified version of the model of Larsen and Sørensen (1987) and propose nucleation in an aphyric basal layer of magma which is supersaturated in all of the mineral phases, but in which nucleation of crystals is inhibited. Following Marsh's (2013) magmatic principles, we infer that the layered kakortokite series did not form through a single chamber filling event and suggest that the basal magma layer formed from a replenishment event. Textural evidence for a replenishment event is observed through resorption of the largest alkali feldspar crystals (Table 1, Fig. 3c–d) in the Unit −1 white kakortokite boundary samples (0–25 mm below Unit 0), which demonstrates a change in the thermal and/or chemical regime between the crystallisation of Unit −1 and the development of Unit 0. Additionally, the upturned kink in all alkali feldspar CSDs, except Location D (Fig. 4c), is indicative of a late-stage nucleation event that formed 'pockets' of small crystals (Fig. 3d). At Locations B and C, there is a small downturned kink between 1.1 to 1.8 mm and 0.9 to 1.4 mm, respectively, providing further evidence for a late-stage nucleation event that overprints previously coarsened crystals. We attribute this to a replenishment event that resulted in melt infiltration into the underlying crystal mush to a depth of less than 30 cm (Fig. 8a).

The eudialyte compositions are consistent with this model as $Fe_{(TOT)}$/Mn ratios have a sharp discontinuity across the Unit −1/Unit 0 boundary (Fig. 7a–b). The $Fe_{(TOT)}$/Mn ratios increase from the U-1 white kakortokite across the Unit −1/Unit 0 boundary to a maximum in the black kakortokite samples from the central regions of the layer (Fig. 7a–b, Table 2). Low eudialyte $Fe_{(TOT)}$/Mn ratios reflect formation from relatively evolved magmas, whereas high $Fe_{(TOT)}$/Mn ratios reflect formation from relatively primitive magmas (Pfaff et al., 2008; Schilling et al., 2011). This indicates that the eudialyte crystals in the Unit 0 black kakortokite crystallised from more primitive magma than those in the underlying Unit −1 white kakortokite, pointing to a change in magma composition at the Unit −1/Unit 0 boundary. Within Unit 0 the $Fe_{(TOT)}$/Mn ratios show a continuous decrease upwards throughout the unit, reflecting crystallisation from a progressively evolving magma.

The additional chemical data from the eudialyte crystals are supportive of an injection of a relatively primitive magma that was halogen-rich. The Ca/(REE + Y) and Cl contents of eudialyte crystals decrease during melt evolution (cf. Pfaff et al., 2008) and all data display a discontinuity at the Unit −1/Unit 0 boundary with the highest ratios in the black kakortokite. The values then decrease upwards continuously through Unit 0 (Fig. 7c–f).

Injection of primitive magma will allow for development of a basal magma layer, due to compositional differences between it and the resident magma. In this model, the resident magma is inferred to have an agpaitic composition and be enriched in incompatible elements but not enriched in volatile elements. The eudialyte compositional data indicate that the injecting magma is richer in iron than the resident magma thus was more primitive and had a greater density. This contributed to pooling of the injected magma between the resident magma and the cumulate pile and to allow downwards percolation into the underlying cumulates. The lack of indicators of magma flow throughout most of the kakortokite series and the planar nature of the unit boundaries reflect an exceptionally quiescent resident magma throughout the development of the layered series, except during the roof collapse event. This reduces the potential for mixing of the injected magma with the resident magma, allowing for the formation of the basal layer. No evidence is found in the present study for xenocrysts within the kakortokites, indicating that the replenishing magma was aphyric. Thus, the injecting magma is inferred to have been saturated in each of the key components (arfvedsonite, eudialyte, alkali feldspar and nepheline) as well as being enriched in volatile elements.

Whilst it is near impossible to determine accurately the thickness of the basal layer that developed each unit, we estimate the scale to be similar to the units. Since the units have a mean thickness of 7 m, we infer that they developed from a basal layer of magma ~10 m thick. It should however be noted that we observe variations in unit thicknesses from 2.5 m to 17 m (measured via drill core) and this may correspond to variations in the volume of injected magma. The resident magma is inferred to have always separated the developing kakortokite sequence from the naujaite, but the magma chamber is inferred to have undergone inflation during development of the rock sequences, thus the resident magma may have had a vertical thickness of a few hundred metres.

The sharp boundary between Unit −1 and Unit 0 formed from combined thermal and chemical erosion of a semi-rigid crystal mush as shown by the embayed alkali feldspar crystals at the unit boundary. Previous authors have noted structures within the layered kakortokites described as slumps (e.g. Bohse et al., 1971). A full description of these rocks and their genesis is outside the scope of the present study, but they do not petrologically or chemically correspond to the kakortokites (Hunt et al., 2014). Thus we infer that Unit −1 was semi-rigid at the time of development of Unit 0, although the roof autolith in Unit +3 indicates that ~20 m of crystal mush was unconsolidated enough to undergo compaction (Larsen and Sørensen, 1987).

The initial high concentration of halogens, as indicated by the Cl-enriched eudialyte crystals in black kakortokite (Fig. 7e–f), will inhibit nucleation of all mineral phases, resulting in supersaturation of each in the magma. As the basal layer of magma cools, due to thermal equilibration, arfvedsonite is the first phase to nucleate (Fig. 9a) as it can crystallise

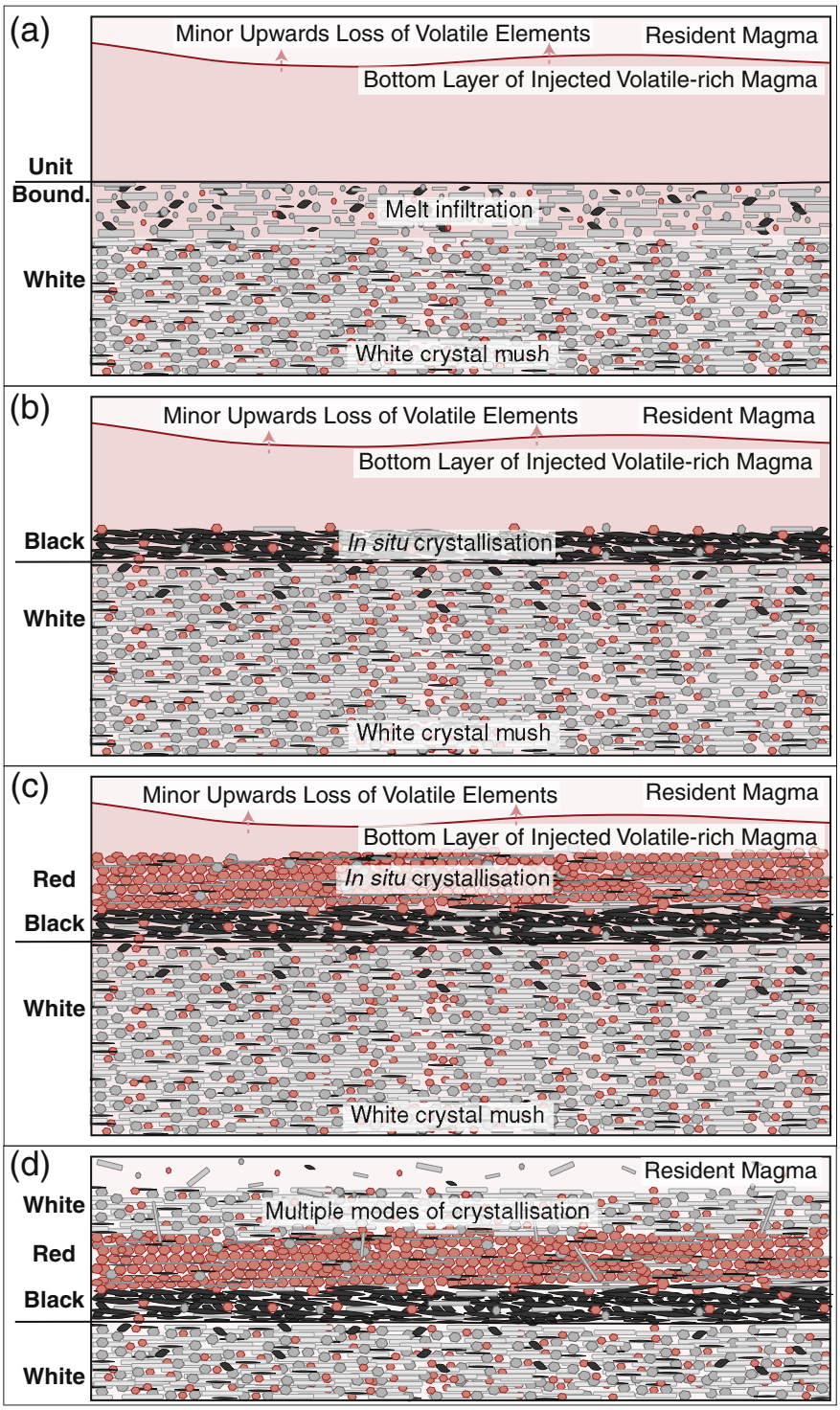

Fig. 8. (a) Injection of a halogen-rich magma at the floor of a quiescent magma chamber results in thermal and/or chemical erosion during downwards infiltration of the melt into the crystal mush. (b) High concentration of halogens in the basal layer of magma inhibits nucleation of all phases except arfvedsonite. (c) Decreasing concentration of halogens allows for crystallisation of eudialyte. (d) Equilibration of the basal magma layer with the resident magma reduces halogen concentrations enough for development of white kakortokite.

at higher concentrations of volatile elements than the other phases (Sørensen, 1969). This main nucleation event of arfvedsonite primarily occurred in situ at the crystal mush–magma interface, potentially enhanced by epitaxial effects, whereas a smaller number of arfvedsonite crystals grew in suspension in the basal layer. Rapid growth, followed by settling of these crystals provided a crystal population that is notably larger than the crystals that grew in situ. These combined processes developed the black kakortokite layer of Unit 0 above the boundary (Fig. 8b) with subordinate crystallisation of the minor phases (alkali feldspar, eudialyte & nepheline).

Crystallisation of the black kakortokite results in a decrease in the concentration of fluorine in the basal magma layer, as crystallisation of arfvedsonite takes F from the magma during crystallisation. Minor processes of upwards loss of halogens along concentration gradients, which

develop as a result of the quiescent state of the resident magma and the coeval crystallisation of the sodalite-rich roof rocks (Larsen and Sørensen, 1987), would also reduce the halogen concentration. This would facilitate the nucleation of eudialyte (Fig. 9b) and a continuous change in halogen concentrations and desaturation in arfvedsonite developed the gradational boundary between the black and red kakortokites (Fig. 9c). Enhanced nucleation of eudialyte primarily occurred in situ at the crystal mush–magma interface, with minor nucleation of the other phases, and developed the red kakortokite.

The concentration of chlorine decreased throughout the formation of red kakortokite. This is due to gradual equilibration of the basal magma layer with the resident magma, through loss of volatile elements due to crystallisation of the Cl-rich eudialyte and minor upward loss along a concentration gradient associated with sodalite crystallisation at the roof of the chamber (Larsen and Sørensen, 1987). This, combined with desaturation of the melt in eudialyte, would allow alkali feldspar and nepheline to nucleate (Fig. 9d), both in suspension in the magma and in situ, developing the white kakortokite above a gradational boundary (Figs. 8d & 9e). This change in primary accumulation method is inferred to be occurring as the basal magma layer equilibrates with the resident magma body. At this stage nucleation occurred in a relatively halogen-poor magma with a density equivalent to the resident magma.

The control on the order of nucleation may be directly related to the halogen content of the magma. High concentrations of halogens depolymerise silicate melts, reducing the length of the silicate chains that can crystallise (e.g. Dingwell et al., 1985). Arfvedsonite has a chain structure (Hawthorne, 1976); eudialyte a ring structure (Johnsen and Grice, 1999); whereas alkali feldspar and nepheline are tectosilicates (Colville and Ribbe, 1968; Tait et al., 2003), thus the silicate connectivity of the mineral structure increases upwards through the unit. As arfvedsonite has the least complex structure, it may nucleate at high concentrations of halogens that inhibit crystallisation of the other phases. Arfvedsonite will take up fluorine from the magma during crystallisation, which would allow for crystallisation of more complex silicates, i.e. eudialyte. Crystallisation of eudialyte will take up chlorine from the melt, which again combined with upwards loss of volatile elements, would then allow alkali feldspar and nepheline to nucleate.

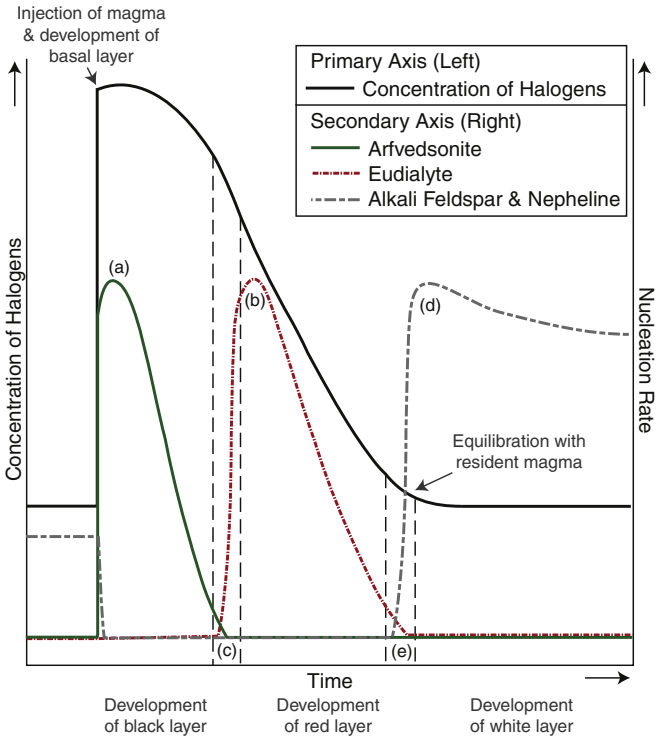

Fig. 9. Speculative kinematic model indicating the effects of varying halogen concentrations on the nucleation of arfvedsonite, eudialyte, alkali feldspar and nepheline.

Although Unit 0 is particularly well developed, the model here can be applied to the entire layered sequence. The present study observes that the general characteristics of each unit are remarkably consistent throughout the entire layered series indicating that each unit formed in a similar manner. Intra-unit chemical variations are described in the present and other studies (e.g. Lindhuber et al., 2015; Pfaff et al., 2008). However, when considering a single layer, e.g. black, red or white, there is very little upwards variation in composition throughout the layered kakortokites (Lindhuber et al., 2015). This consistency is ascribed in our model to replenishment by magmas with minimal compositional variations, allowing for crystallisation of units with similar chemical compositions. The discontinuities at unit boundaries between the underlying white kakortokite and overlying black kakortokite reflect replenishment events. The exact number of replenishment events required to develop the entire series is uncertain, but could be as many as 29, i.e. 1 per unit. Each unit in the model accretes upwards, through both in situ growth and accumulation through gravitational settling, with each unit building up from the underlying. Accumulation of the overlying units will compact the underlying units and contribute to the textural development through enhancing fabric development.

6. Conclusions

CSD data are inconsistent with gravitational settling as the primary mode through which the macrorhythmic layering developed. Instead, in situ crystallisation (black and red kakortokite) and in situ crystallisation combined with density segregation, i.e. settling and flotation (white kakortokite) were the key processes that developed Unit 0. The key control on unit development was an oscillating volatile element concentration, which decreased during the development of a unit and sharply increased at the boundary to the next. An open-system model is proposed whereby a replenishment event formed Unit 0. An initial high concentration of volatile elements allowed for the formation of the black kakortokite through nucleation of arfvedsonite, whereas nucleation of the other phases was suppressed. This nucleation combined with the minor processes of equilibration of the basal magma layer with the resident magma and upwards loss of volatiles along concentration gradients to the roof, decreased the concentration of halogens. This enabled development of red and then white kakortokite above gradational boundaries from the underlying layer. This alternative nucleation model, controlled by variations in volatile element concentration, has been debated (Bailey et al., 2006; Larsen and Sørensen, 1987). However, our approach of combining field analysis and detailed petrographic studies with quantitative textural and mineral chemical analyses provides more data to support the hypothesis. The final textures observed in Unit 0 indicate that late-stage grain growth occurred through overgrowth, i.e. intercumulus enlargement, and processes of textural coarsening. This was promoted through variations in the degree of undercooling throughout the cooling history of Unit 0. It resulted in modification of the primary CSD profiles. Although Unit 0 is particularly well developed, the model presented here may be generally applicable to the entire sequence of layered kakortokite as the general characteristics of each unit are remarkably consistent.

This study provides greater insight into the magma chamber dynamics operating during the formation of the kakortokite, as open system behaviour is indicated with periodic injections of magmas that are more primitive than the resident magma. Ilímaussaq is arguably the most celebrated agpaitic body, but these processes may be important to understanding the origins of other layered agpaitic rocks, e.g. Lovozero, Russia; Nechalacho, Canada; and Pilanesberg, South Africa.

Supplementary data to this article can be found online at http://dx.doi.org/10.1016/j.lithos.2016.10.023.

Acknowledgements

We thank TANBREEZ Mining Greenland A/S for their assistance with fieldwork, sampling and access to the complex and drill core. Michael Higgins and Brian Upton are thanked for their thorough reviews, which greatly improved the manuscript. Allen Glazner is thanked for his thoughtful comments on an earlier version. EJH acknowledges funding from a NERC PhD studentship and the work was completed at the University of St Andrews, UK.

References

Armstrong, J.T., 1991. Quantitative Elemental Analysis of Individual Microparticles with Electron Beam Instruments, Electron Probe Quantitation. Springer, pp. 261–315.
Bailey, J.C., Sørensen, H., Andersen, T., Kogarko, L.N., Rose-Hansen, J., 2006. On the origin of microrhythmic layering in arfvedsonite lujavrite from the Ilímaussaq alkaline complex, South Greenland. Lithos 91, 301–318.
Bohse, H., Brooks, C.K., Kunzendorf, H., 1971. Field observations on the kakortokites of the Ilimaussaq intrusion, South Greenland, including mapping and analyses by portable X-ray fluorescence equipment for zirconium and niobium. Rapport. Grønlands Geologiske Undersøgelse 38 (43 pp.).
Bons, P.D., Baur, A., Elburg, M.A., Lindhuber, M.J., Marks, M.A.W., Soesoo, A., van Milligen, B.P., Walte, N.P., 2015. Layered intrusions and traffic jams. Geology 43, 71–74.
Boorman, S., Boudreau, A., Kruger, F.J., 2004. The lower zone–critical zone transition of the Bushveld Complex: a quantitative textural study. Journal of Petrology 45, 1209–1235.
Borst, A.M., Friis, H., Andersen, T., Nielsen, T.F.D., Waight, T.E., Smit, M.A., 2016. Zirconosilicates in the kakortokites of the Ilímaussaq complex, South Greenland: implications for fluid evolution and high-field-strength and rare-earth element mineralization in agpaitic systems. Mineralogical Magazine 80, 5–30.
Brothers, R.N., 1964. Petrofabric analyses of Rhum and Skaergaard layered rocks. Journal of Petrology 5, 255–274.
Cabane, H., Laporte, D., Provost, A., 2005. An experimental study of Ostwald ripening of olivine and plagioclase in silicate melts: implications for the growth and size of crystals in magmas. Contributions to Mineralogy and Petrology 150, 37–53.
Cashman, K.V., Marsh, B.D., 1988. Crystal size distribution (CSD) in rocks and the kinetics and dynamics of crystallization II: Makaopuhi lava lake. Contributions to Mineralogy and Petrology 99, 292–305.
Colville, A.A., Ribbe, P.H., 1968. The crystal structure of an adularia and a refinement of the structure of orthoclase. The American Mineralogist 53, 25–37.
DeHoff, R.T., 1991. A geometrically general theory of diffusion controlled coarsening. Acta Metallurgica et Materialia 39, 2349–2360.
Dingwell, D.B., Scarfe, C.M., Cronin, D.J., 1985. The effect of fluorine on viscosities in the system Na_2O–Al_2O_3–SiO_2: implications for phonolites, trachytes and rhyolites. American Mineralogist 70, 80–87.
Ferguson, J., 1964. Geology of the Ilímaussaq alkaline intrusion, South Greenland. Part I. Description of map and structure. Meddelelser om Grønland 172, 1–81.
Hawthorne, F.C., 1976. The crystal chemistry of the amphiboles: V. The structure and chemistry of arfvedsonite. Canadian Mineralogist 14, 346–356.
Higgins, M.D., 1991. The origin of laminated and massive anorthosite, Sept Iles intrusion, Quebec, Canada. Contributions to Mineralogy and Petrology 106, 340–354.
Higgins, M.D., 1998. Origin of anorthosite by textural coarsening: quantitative measurements of a natural sequence of textural development. Journal of Petrology 39, 1307–1323.
Higgins, M.D., 1999. Origin of megacrysts in granitoids by textural coarsening: a crystal size distribution (CSD) study of microcline in the Cathedral Peak Granodiorite, Sierra Nevada, California. In: Castro, A., Fernández, C., Vigneresse, J.L. (Eds.), Understanding Granites: Integrating New and Classical Techniques. Geological Society London, Special Publications, London, pp. 207–219.
Higgins, M.D., 2000. Measurement of crystal size distributions. American Mineralogist 85, 1105–1116.
Higgins, M.D., 2002a. Closure in crystal size distributions (CSD), verification of CSD calculations, and the significance of CSD fans. American Mineralogist 87, 171–175.
Higgins, M.D., 2002b. A crystal size-distribution study of the Kiglapait layered mafic intrusion, Labrador, Canada: evidence for textural coarsening. Contributions to Mineralogy and Petrology 144, 314–330.
Higgins, M.D., 2006. Quantitative Textural Measurements in Igneous & Metamorphic Petrology. Cambridge University Press, Cambridge.
Higgins, M.D., 2010. Imaging birefringent minerals without extinction using circularly polarized light. The Canadian Mineralogist 48, 231–235.
Higgins, M.D., 2011. Textural coarsening in igneous rocks. International Geology Review 53, 354–376.
Holness, M.B., Cheadle, M.J., McKenzie, D., 2005. On the use of changes in dihedral angle to decode late-stage textural evolution in cumulates. Journal of Petrology 46, 1565–1583.
Hunt, E.J., Finch, A.A., Donaldson, C.H., 2014. Magma mixing in layered kakortokites — Ilímaussaq Complex. S. Greenland, AGU Fall Meeting, San Francisco.
Johnsen, O., Ferraris, G., Gault, R.A., Grice, J.D., Kampf, A.R., Pekov, I.V., 2003. The nomenclature of eudialyte-group minerals. The Canadian Mineralogist 41, 785–794.
Johnsen, O., Grice, J.D., 1999. The crystal chemistry of the eudialyte group. Canadian Mineralogist 37, 865–891.
Larsen, L.M., Sørensen, H., 1987. The Ilímaussaq intrusion — progressive crystallisation and formation of layering in an agpaitic magma. Geological Society of London, Special Publication 30, 473–488.
Lauder, W.R., 1964. 'Mat' formation and crystal settling in magma. Nature 202, 1100–1101.
Lindhuber, M.J., Marks, M.A.W., Bons, P.D., Wenzel, T., Markl, G., 2015. Crystal mat-formation as an igneous layering-forming process: textural and geochemical evidence from the 'lower layered' nepheline syenite sequence of the Ilímaussaq complex, South Greenland. Lithos 224, 295–309.
Marks, M.A.W., Markl, G., 2015. The Ilímaussaq Alkaline Complex, South Greenland. In: Charlier, B., Namur, O., Latypov, R., Tegner, C. (Eds.), Layered Intrusions. Springer Geology, Dordrecht, pp. 649–691.
Marsh, B.D., 1988. Crystal size distribution (CSD) in rocks and the kinetics and dynamics of crystallization I. Theory. Contributions to Mineralogy and Petrology 99, 277–291.
Marsh, B.D., 1998. On the interpretation of crystal size distributions in magmatic systems. Journal of Petrology 39, 553–599.
Marsh, B.D., 2013. On some fundamentals of igneous petrology. Contributions to Mineralogy and Petrology 166, 665–690.
McNown, J.S., Malaika, J., 1950. Effects of particle shape on settling velocity at low Reynolds numbers. Transactions — American Geophysical Union 31, 74–82.
Meurer, W.P., Boudreau, A.E., 1998. Compaction of igneous cumulates part II: compaction and the development of igneous foliations. The Journal of Geology 106, 293–304.
Mock, A., Jerram, D.A., 2005. Crystal size distribution (CSD) in three dimensions: insights from the 3D reconstruction of a highly porphyritic rhyolite. Journal of Petrology 46, 1525–1541.
Morgan, D.J., Jerram, D.A., 2006. On estimating crystal shape for crystal size distribution analysis. Journal of Volcanology and Geothermal Research 154, 1–7.
Parsons, I., Butterfield, A.W., 1981. Sedimentary features of the Nunarssuit and Klokken syenites, S Greenland. Journal of the Geological Society 138, 289–306.
Pfaff, K., Krumrei, T., Marks, M.A.W., Wenzel, T., Rudolf, T., Markl, G., 2008. Chemical and physical evolution of the 'lower layered sequence' from the nepheline syenitic Ilímaussaq intrusion, South Greenland: implications for the origin of magmatic layering in peralkaline felsic liquids. Lithos 106, 280–296.
Pfaff, K., Wenzel, T., Schilling, J., Marks, M.A.W., Markl, G., 2010. A fast and easy-to-use approach to cation site assignment for eudialyte-group minerals. Neues Jahrbuch Fur Mineralogie-Abhandlungen 187, 69–81.
Schilling, J., Wu, F.-Y., McCammon, C., Wenzel, T., Marks, M.A.W., Pfaff, K., Jacob, D.E., Markl, G., 2011. The compositional variability of eudialyte-group minerals. Mineralogical Magazine 75, 87–115.
Simakin, A.G., Bindeman, I.N., 2008. Evolution of crystal sizes in the series of dissolution and precipitation events in open magma systems. Journal of Volcanology and Geothermal Research 177, 997–1010.
Sørensen, H., 1969. Rythmic igneous layering in peralkaline intrusions: an essay review on Ilímaussaq (Greenland) and Lovozero (Kola, USSR). Lithos 2, 261–283.
Sørensen, H., 1997. The agpaitic rocks - an overview. Mineralogical Magazine 61, 485–498.
Sørensen, H., 2001. Brief introduction to the geology of the Ilímaussaq alkaline complex, South Greenland, and its exploration history. In: Sørensen, H. (Ed.), The Ilímaussaq Alkaline Complex, South Greenland: Status of Mineralogical Research With New Results. Geology of Greenland Survey Bulletin, Copenhagen.
Steenfelt, A., Bohse, H., 1975. Variations in content of uranium in eudialyte from differentiated alkaline Ilimaussaq intrusion, South Greenland. Lithos 8, 39–45.
Tait, K.T., Sokolova, E., Hawthorne, F.C., 2003. The crystal chemistry of nepheline. The Canadian Mineralogist 41, 61–70.
Upton, B.G.J., 1961. Textural features of some contrasted igneous cumulates from South Greenland. Meddelelser om Grønland 123, 1–29.
Upton, B.G.J., 2013. Tectono-magmatic evolution of the younger Gardar southern rift, South Greenland. Geological Survey of Denmark and Greenland Bulletin 29, 124.
Upton, B.G.J., Emeleus, C.H., Heaman, L.M., Goodenough, K.M., Finch, A.A., 2003. Magmatism of the mid-Proterozoic Gardar Province, South Greenland: chronology, petrogenesis and geological setting. Lithos 68, 43–65.
Upton, B.G.J., Parsons, I., Emeleus, C.H., Hodson, M.E., 1996. Layered alkaline igneous rocks of the Gardar Province, South Greenland. In: Cawthorn, R.G. (Ed.), Layered Intrusions. Elsevier Science, Amsterdam, pp. 331–363.
Ussing, N.V., 1912. Geology of the country around Julianehaab, Greenland. Meddelelser om Grønland 38, 1–426.
Waight, T., Baker, J., Willigers, B., 2002. Rb isotope dilution analyses by MC-ICPMS using Zr to correct for mass fractionation: towards improved Rb–Sr geochronology? Chemical Geology 186, 99–116.